Research Square

Preprints are preliminary reports that have not undergone peer review.
They should not be considered conclusive, used to inform clinical practice,
or referenced by the media as validated information.

Effect of Dopant Concentrations on Sensing Properties of Ni Doped TiO 2 based Resistive Humidity Sensor

Dipak Gapale
Sangamner Nagarpalika Arts, D. J. Malpani Commerce and B. N. Sarda Science College (Autonomous), Sangamner

Pravinkumar Jadhav
Sangamner Nagarpalika Arts, D. J. Malpani Commerce and B. N. Sarda Science College (Autonomous), Sangamner

Sainath Navale
Sangamner Nagarpalika Arts, D. J. Malpani Commerce and B. N. Sarda Science College (Autonomous), Sangamner

Sandeep Arote
Sangamner Nagarpalika Arts, D. J. Malpani Commerce and B. N. Sarda Science College (Autonomous), Sangamner

Balasaheb Palve
Sangamner Nagarpalika Arts, D. J. Malpani Commerce and B. N. Sarda Science College (Autonomous), Sangamner

Prashant Baviskar
pkbaviskar@sangamnercollege.edu.in

Sangamner Nagarpalika Arts, D. J. Malpani Commerce and B. N. Sarda Science College (Autonomous), Sangamner

Research Article

Keywords: Thin films, Ni doped TiO2, Spray pyrolysis, Electrical and Optical properties, Humidity sensor

Posted Date: November 10th, 2026

DOI: https://doi.org/10.21203/rs.3.rs-10982732/v1

License: This work is licensed under a Creative Commons Attribution 4.0 International License.
Read Full License

Additional Declarations: No competing interests reported.

Effect of Dopant Concentrations on Sensing Properties of Ni Doped TiO_2 based Resistive Humidity Sensor

Dipak L. Gapale, Pravinkumar D. Jadhav, Sainath R. Navale, Sandeep A. Arote, Balasaheb M. Palve[*] *and Prashant K. Baviskar*[*]

Department of Physics, Sangamner Nagarpalika Arts, D. J. Malpani Commerce and B. N. Sarda Science College (Autonomous), Sangamner 422605 (M.S.) India

Abstract

In the present work, effect of different volume percentages (*vol %*) of Ni doped TiO_2 thin films on structural, microstructural, electrical, optical and humidity sensing properties were investigated. The pristine TiO_2 and Ni doped TiO_2 thin films were synthesized for different *vol%* of Ni dopants such as 1 *vol%*, 2 *vol%* and 4 *vol%.* onto the glass substrate using spray pyrolysis technique. Structural properties of synthesized sample showed polycrystalline anatase tetragonal phase with dominant (101) peak. Electrical resistance of the samples also decreased with increase in dopant concentration. Temperature coefficient of resistance and activation energy shows strong correlation with dopant concentration. The optical band gap of the samples also decreased with rise in Ni dopant *vol%* up to 2, but further rise in concentration it increased for 4 *vol%*. The maximum humidity sensitivity of 89% was observed for the sample with 2 *vol%* of Ni doped TiO_2 with low response time of 64 s.

Keywords: Thin films; Ni doped TiO_2; Spray pyrolysis; Electrical and Optical properties; Humidity sensor.

[*]Corresponding authors: palve@sangamnercollege.edu.in (BMP);
pkbaviskar@sangamnercollege.edu.in (PKB)

Introduction

Metal oxide nanomaterials are widely used due to significant properties like high mechanical stress, high dielectric constants, tuneable structure, easily synthesized and abundant in nature [1]. Titanium dioxide (TiO_2) is one of the extensively studied compound from this group due to significant material properties for the application in dye-sensitized solar cell [2], photocatalyst [3], microwave absorption [4], and variety of sensors [5]. Due to the high hydrophilicity and chemical stability, TiO_2 were usually studied as humidity sensor application [6]. TiO_2 nanomaterials with different shapes and structures like nano-rods [7], nanoparticles [8], nano-flowers [8], nano-wires [8], nanotubes [9], nanocubes [10], nanobelts [11] etc., have been synthesized to increase the surface area of the material for improved detection of water molecules.

In literature, various physicals and chemical methods have been introduced to synthesize the TiO_2 nanostructures [12]. The various chemical methods have been used to deposit pristine TiO_2, metal doped TiO_2 and metal oxide composite TiO_2 such as sol-gel, hydrothermal, SILAR, chemical bath deposition, spray pyrolysis etc., Among this spray pyrolysis technique is largely studied due to its simplicity, easy handling, multi-composite film deposition ability along with low-cost synthesis of thin films with a larger surface area.

In the present paper, a modified spray pyrolysis technique has been used, as it offers a precise control on various synthesis parameters like substrate temperature, air to fluid flow rate (AFR), substrate to nozzle distance, atmosphere, precursor concentration, film thickness etc. [13]. Increase in the available adsorption sites have improved the sensor response and thus various metal ions were doped into pristine materials. Transition metal ions or their oxides are used as a dopant into pristine TiO_2 as their ionic radii are comparable and have variable oxidation states. The transition metal ions can significantly alter the properties such as crystalline structure, size and shape of nanomaterials, surface morphology, optical band gap, surface to volume ratio etc. Earlier studies on doped TiO_2 reported that, the properties like electrical (enhances charge carrier separation) [14], optical (reduction in band gap) [15], photochromic (change in color with the incoming light) [16], surface (change in surface oxygen vacancies) [17], structural (anatase to rutile phase transition) [18] are altered due to metal dopants. Dopants like Mn, Fe

and Ni have shown mixed phases in the compounds, whereas the transition metal dopants like Cu, Cd, V, Cr, Zn, Co, etc. have reported to stimulate the phase transformation from anatase to rutile [14]. Nickel (Ni) can alter the properties of TiO_2 as the ionic radius of Ni (0.74 Å) is very close to that of Ti^{4+} (0.68 Å), which makes the doping easy. Nickel doping can change the band gap energy of TiO_2 due to the introduction of intermediate band gap state [19]. Ni doping in pristine TiO_2 can also modify material morphology [20], enhance photocatalysis [21] Ni doped TiO_2 offers more active sites due to the formation of more oxygen vacancies on the surface of the material [22], UV light-induced hydrophilicity [23] etc. Generally, the materials with high hydrophilicity were used for humidity sensing applications [24].

In literature, metal doping in to pristine TiO_2 have reported to increase the humidity sensor response. Li *et al.* [25] have reported the improvement of sensitivity with lower response time of 24 s for cobalt (Co) doping of ordered mesoporous TiO_2. Musa *et al*. [26] have reported rise in sensitivity owing to the increased defect sites, namely oxygen vacancies related to the V doped TiO_2. Pandey e*t al* [27] reported lower response and recovery time of 84 s and 396 s, respectively, for ZnO-TiO_2 nanocomposite. However, to the best of our knowledge, Ni doped TiO_2 has not yet been tested for the humidity sensor application. In the present work, an attempt has been made to improve the humidity sensor sensitivity with Ni doped into TiO_2 lattice.

Experimental

Ni doped TiO_2 samples were successfully synthesized onto glass substrates for different dopant *vol%* using modified spray pyrolysis technique. The precursor solutions used include the analytical grade Titanium Tri-Chloride ($TiCl_3$; Sigma Aldrich) and Nickel(II) Chloride Hexahydrate ($NiCl_2.6H_2O$; Sigma Aldrich). The concentrations of both the precursor solutions were adjusted to 0.1 M in order to control Ni *vol%*. These two precursor solutions were mixed vigorously at room temperature using magnetic stirrer. With variation in volume percentage, the atomic weight percentage of Ni dopant can be changed. Other spray process parameters such as deposition temperature (350 ^oC), distance between spray gun to substrate (30 cm), solution flow rate (1 mℓ per minute), carrier air flow rate (7.5 ℓpm) were

kept constant during the deposition. All the deposited films were then annealed at 500 ºC for 2 hrs in an air atmosphere.

The phase formation was confirmed by X-ray diffraction (XRD) pattern obtained using a BRUKER D8 ADVANCE diffractometer (Japan, Rigaku, D/Max 2500PC) with Cu-Kα (λ=0.15418 nm). The morphological and elemental analysis were carried out by using scanning electron microscopy (SEM) with a JEOL-540LV microscope. The electrical and humidity sensing measurements were done by using an *in-situ* set up designed for resistance measurement. Humidity sensing properties of the deposited material were recorded by measuring the film resistances as a function of change in relative humidity. Humidity meter (MEXTECH, model no. M288CTHW) was used to record relative change in humidity.

Results and Discussion

X Ray Diffractometry (XRD)

Figure 1 shows XRD spectra of the pristine and Ni doped TiO_2 thin films annealed at 500 ºC temperature for 2 hrs with various Ni volume percentage (*vol%*). XRD pattern shows narrow peaks corresponding to (101), (004), (200), (105), (211), (204) and (116) crystalline planes for the pristine TiO_2 film. These peaks confirm the polycrystalline anatase TiO_2 with tetragonal phase and lattice parameters as (a ~ 3.7853 Å, c ~ 9.5138 Å). Observed results are in good agreement with the standard JCPDS (# 21-1272) data for pristine TiO_2 films. The XRD patterns for 1 *vol%*, 2 *vol%* and 4 *vol%* Ni doped TiO_2 thin film samples shows that the intensity of prominent peak indexed to (101) plane decreases and peak broadening increases as the concentration of Ni dopant increases. The crystallite size was found to be decrease as increase in Ni dopant concentration. However, the intensity of the (004) peak increases with reduction in peak broadening that results in increase in crystallite size for 4 *vol%* doped TiO_2 sample. No other peaks corresponding to Ti or other impurities like Ni, NiO, $NiTiO_3$, mixed anatase and rutile phase as well as rutile phase of TiO_2 were found even at higher Ni concentrations (up to 4 *vol%*), which indicates successful doping of Ni. This is attributed the ionic radius (~69 pm) of Ni^{2+} [28] which is comparable to that of Ti^{4+} (~68 pm) and can also form octahedral coordination like Ti^{4+} [29].

The distinguished structural parameters such as crystallite size, micro-strain and specific surface area were calculated by using appropriate formulae as discussed in earlier report [30]. Crystallite sizes are calculated from Scherrer's formula and the values are tabulated in table 1 for pristine and Ni doped TiO_2 samples. With increase in Ni dopant, it was observed that there was no distinguishable change in Bragg positions, but the strength of diffraction peak was affected due to Ni dopant atoms. The intensity of the diffraction peak decreases with increase in concentration of Ni dopant up to 2 *vol%* . This result indicate that decrease the material crystallinity with Ni doping. Furthermore, the increase in Ni concentration causes the enhancement in intensity of (004) diffraction peak. The inconsistent change in the crystallite size is attributed to the lattice strains produced during growth of the films. Crystallite size increases at higher concentration of Ni due to decrease in micro-strain [29, 31]. Micro-strain values for the pristine and Ni doped TiO_2 samples were calculated, which is increased with increase in Ni dopant concentration and showed decrease for higher Ni concentration (4 *vol%*). The specific surface area of pristine and Ni doped TiO_2 films were found to increase with increase in concentration of Ni, which indicates increase in crystal lattice defects [32]. Increase in micro-strain can sizably reduce the crystallite size and enhance surface area of the films. Increase in specific surface area can then improve the surface activity of the Ni doped TiO_2 thin films. The surface-active sites can enhance the sensing properties of the material.

Scanning Electron Microscopy (SEM)

The SEM images of the pristine and Ni doped TiO_2 samples presented in figure 2 show interconnected weblike morphology with particles and micropores attached to the interconnected webs. The agglomerated particles break to form a flower like morphology for Ni doped samples with 1 *vol%* and 2 *vol%* which enhances the surface area of the deposited films. The increase in surface area improves the surface adsorbed site as well as surface activity which is adventitious in sensing applications. With further increase in Ni concentration, opening of the micropores gets blocked due to agglomeration of the nanoparticles which reduces the surface area of material and thus film shows a dense structure. Open and close endings of surface pores have special importance for the sensing and photocatalytic applications. Surfaces with open end pores have advantage due to the enhancement in surface area which can improve the sensing performance [33].

Energy dispersive spectroscopy (EDX)

Energy dispersive spectroscopy (EDX) technique was employed for elemental analysis of pristine and Ni doped TiO_2 thin films. The EDX spectra for pristine and Ni doped TiO_2 thin films with various Ni concentrations are presented in figure 3 and the elemental compositions are tabulated in table 2. EDX spectra show the peaks corresponding to Ti (energy ~ 4.5 keV), O (energy ~ 0.525 keV), Ni (energy ~ 7.471 keV) and Si (energy ~ 1.739 keV) without any other peaks, which suggests that the synthesized samples consist of Ti, Ni, and O elements from Ni doped TiO_2 thin films. The peak corresponding to Si in EDX spectrum is due to the use of silica substrate for the thin film deposition.

Optical Properties

The optical properties of pristine and Ni doped TiO_2 thin films were investigated using UV-Vis spectrophotometer in the wavelength range 200 nm to 800 nm. The strong correlation between Ni dopant *vol%* and optical absorption was observed, which shows reduction in absorption with rise in Ni dopant *vol%*. The optical absorption edge was observed to sharp and shifted towards red end (higher wavelength region) with 2 *vol%* and further increase in Ni concentration results in decrease in the wavelength. The optical band gap of the film samples can be calculated from the Tauc plots of $(absorbance)^2$ Vs hυ [34] shown in figure 4. The schematic energy level diagram for pristine and Ni doped TiO_2 is depicted in figure 4 (inset). In present study the small reduction in energy band gap with increasing Ni concentration may be due to decreasing sp-d hybridization energy. Where **s** orbital is from Oxygen element and **p** orbital is from Titanium element of TiO_2 and **d** orbital is from Nickle element.

Direct optical band gap of the pristine and Ni doped TiO_2 thin film samples were observed to decrease with change in *vol%* Ni doping leads to the red shift. The observed values of the direct band gap of pristine and Ni doped TiO_2 samples were reported in table 2, which may be related to Ni^{2+} impurity band present between conduction and valence band of TiO_2 [35]. Nishikawa *et al.* [36] have attributed the reduction in band gap to the comparable ionic radii of Ni^{2+} and Ti^{4+}, therefore, Ni^{2+} form octahedral coordination like Ti^{4+}.

Electrical Properties

The electrical properties of the synthesis samples were investigated with two probe method. The electrical resistance film samples were measure using Keithley multimeter 2000. The electrical properties like resistance, temperature coefficient of resistance and activation energy were investigated by measuring resistance of the film samples as a function of temperature. It is observed that the resistance of pristine and Ni doped TiO_2 films decreased with increase in the Ni dopant concentration, which confirms semiconducting behaviour of the film samples. The electrical resistance for pristine and Ni doped TiO_2 thin films is presented in table 3. The native donor concentrations get reduced due to heating in air, which is responsible for reduction in resistance of the films. Thermal sensitivity of a material can be represented in terms of temperature coefficient of resistance and activation energy. Temperature coefficient of resistance of the samples under investigations was calculated from the log (R_a) Vs temperature curves [37] as presented in figure 5.

Negative value of the TCR for Ni doped TiO_2 shows negative temperature coefficient of resistance (NTC). As, Ni dopant concentration is increased, TCR was observed to increase from -0.0014 C^{-1} to -0.0005 C^{-1} as presented in table 3.

Arrhenius plots were used to determine activation energy of the synthesized samples, which indicates that Ni dopant concentration enhance the activation energy of the samples as shown in figure 6. Calculated activation energy was observed to increase from 0.34 eV to 0.66 eV for cooling cycle with increase in Ni dopant level as tabulated in table 3. The rise in activation energy is due to existence of activation of the working level of nickel doping into TiO_2.

Humidity Sensing Properties

The humidity sensing properties of Ni doped TiO_2 films were investigated by measuring change in resistance of the film with corresponding change in relative humidity at room temperature. It is observed that the resistance of the film sample decreases quickly when humidity changes in the lower range. Figure 7 displays the variation of resistance of the film samples with change in percentage of relative humidity (% RH).

The rate of change of resistance with relative humidity is observed to be maximum at lower relative humidity and minimum at higher relative humidity, which confirms the nonlinear relationship. Decrease in resistance of the film samples with relative humidity indicates enhancement in electrical conduction when water molecules get adsorbed on the film surface. Increase in electrical conductance with relative humidity is due to the chemisorbed hydroxyl ions on the surface of the sensor material which can either donate electrons to conduction band or through proton ($H^{+)}$ hopping between hydroxyl groups [38]. In chemisorbed layer, the water vapour dissociates into hydroxyl group (OH^-) and hydrogen group (H^+) on the surface of the film samples. Thus, the hydroxyl group gets attracted towards Ti^{3+} atom and H^+ group towards oxygen species or pre-adsorbed oxygen species on the surface of the sample due to this the barrier potential alters and which causes the reduction in resistance of the sample [39]. More oxygen vacancies on the surface of the sample give a more active absorption site for the water vapours. With doping of Ni^{2+}, the oxygen vacancies on the surface of the sample increased. Therefore, the increase in Ni doping led to enhancement in water vapour absorption on the surface causing the formation of H_3O^+ ions, which increase the conductivity of Ni doped TiO_2 sample; similar results were reported for Fe doped SnO_2 [40]. Furthermore, increase in relative humidity leads to physisorbed water molecules on hydroxyl layer. Significance of the physisorbed layer lies in the cation charge developments from sensor material or the impurities present in materials and the water molecules present on the surface of the sensor material [41]. First physisorbed layer is formed between hydroxyl layer and water molecules adsorbed on it, bounded by hydrogen double bonds. With further increase in relative humidity, second physisorbed layer is formed between the first physisorbed water molecules and the water molecules on its surface. In first and second physisorbed layers, the transfer of proton (H^+ ions) from one water molecule to another take place. Thus, the conduction takes place due to proton hopping between water molecules; which is called as Grotthuss conduction mechanism [42].

Sensitivity of a sensor is defined as the ratio of difference in resistance between dry and humid conditions to the resistance at dry condition [43].

$$S = \frac{R_H - R_D}{R_D} \times 100\ \% \qquad \text{---------(1)}$$

Sensitivity of a sensor is expressed in terms of the percentage of sensitivity. Sensitivity of pristine and Ni doped TiO_2 samples were determined by measuring resistance in dry air and in humid condition. In the present case, sensitivity of the film samples was observed to increase with increase in relative humidity. At higher relative humidity, sensitivity of the pristine and Ni doped TiO_2 samples was found to change slowly or were nearly constant, as shown in figure 8. 2 *vol%* Ni doped TiO_2 sample shows higher sensitivity of about 89% than that of the other samples. Sensitivity was decreased for higher Ni concentrations (4 *vol%* Ni), which was 80.5%. Increase in sensitivity was observed with Ni dopant concentration from 0 *vol%* to 2 *vol%* and then it showed a declination. Hysteresis curves of pristine and Ni doped TiO_2 thin films are presented in figure 8. Data on hysteresis for the synthesized samples was obtained by measuring sensitivity of the samples during humidification and dehumidification process. The hysteresis loss can be expressed in terms of percentage of hysteresis which can be calculated using the relation [43].

$$\%\ \text{of Hysteresis} = \left[\frac{R_{dehumid} - R_{humid}}{R_{max} - R_{min}}\right] \times 100\% \quad \text{----------(2)}$$

Where, $R_{dehumid}$ is resistance at mean value of percent relative humidity (PRH) of the sample during dehumidification, R_{humid} is resistance at mean value of PRH of the sample during humidification, R_{max} is the resistance at maximum PRH and R_{min} is the resistance at minimum PRH.

Percentage of hysteresis loss is a key parameter for selection of the humidity sensor, which is related to the stability, reliability and selectivity. If the percentage of the hysteresis is smaller than 5 % then the sensor has good selectivity. In present case, the percentage of hysteresis loss was found to increase with the Ni dopant concentration. Maximum percentage of hysteresis loss as 6.37% was reported for sample 4 *vol%* of Ni, as presented in table 4. Hysteresis loss for the pristine sample is less; which indicates that the pristine sample must have excellent stability, reliability and good selectivity among all other samples. However, the hysteresis losses for the other samples were also very low i.e., below 5% except 4 *vol%* Ni doped TiO_2 sample, so they must have good stability, reliability and selectivity.

Response time of a sensor is the time required to achieve 90% of the total resistance change for humidification/adsorption process. The recovery time is time required to achieve 90% of the total

resistance change for dehumidification/desorption process. Figure 9 shows variations of change in resistance with corresponding change in time which presents response and recovery time for the pristine and Ni doped TiO_2 samples.

The response time was found to change with change in Ni dopant concentrations. The minimum response time of 64.5 s was obtained for the 2 *vol%* of Ni doped TiO_2 sample. The response time was found to be increase further increase in Ni doping concentration. The recovery times for all the samples were very small; around 3 s to 4.5 s as shown in table 4. Literature shows reports on Co [44], N [45] and KCl [46] doped TiO_2 samples to have good sensitivity represented in terms of R_{air}/R_{humid} and a maximum sensitivity of order of 10^4. In the present case, resistance of the 2 *vol%* Ni doped TiO_2 sample changes from 9 GΩ to 1.2 MΩ which gives a sensitivity of about 7.8×10^3. The recovery time for the above cited compositions is higher than the present case. The Ni doped TiO_2 films exhibit smaller response and recovery time of 64.5 s and 3 s respectively.

Morphology of the sensing material plays an important role, which is responsible for the amount of water vapours adsorbed and desorbed on its surface [47]. Presence of pores and their distribution over the surface of the sample considerably affects the sample sensitivity and is ascribed to the change in surface area. During the humidification process, water vapours on the surface of the sensing sample shows strong correlation with size of the pores and their distribution. The open or closed pore surface has its own contribution in humidity sensitivity. Open pores have the advantage of capillary conduction mechanism, which can enhance sensitivity of the material [48]. Closed pores reduce the surface area which then reduces adsorption of water vapours and reduce the sensitivity of the sensing sample. Formation of chemisorbed and physisorbed layers can also get affected by pore size and their distribution on the surface of the sensing samples [49]. Thus, getting optimum size micro-pores is a notable success for better humidity sensing performance. The humidity sensing mechanism at room temperature is of ionic type [37]. In the present study, it was observed that sensitivity of the Ni doped TiO_2 samples increases with increase in Ni dopant level, which can be attributed to the increase in charge carriers due to doping. The sample synthesized at 2 *vol%* of Ni showed more micro pores along with splitting of grains which can also improve porosity of the material and exhibit higher sensitivity. The surface acceptor sites also

increase due to the increase in charge carrier with increase in Ni doping. Thus, the sensitivity increases with Ni dopants concentration. The highest sensitivity of 89 % was recorded for 2 *vol%* Ni doped TiO_2 sample. Further, increase in Ni dopants to 4 *vol%*, could elevate the charge concentration as well as surface acceptor sites, facilitating enhancement in sensitivity. It can be seen from the morphology micrographs that, at this dopant concentration (4 *vol%*), the film sample is dense and have some cracks which may can be responsible for reduction in sensitivity of the sample. The complete results on humidity sensitivity and response time of the samples vary with the Ni *vol%* and are presented in figure 10. This result clearly indicate that the optimized Ni dopant *vol%* for better humidity sensing performance is 2 *vol%*. With increase in micro-strain and specific surface area, the sensitivity of the synthesis Ni doped TiO_2 samples increases. Also, with increase in amount of Ni, the structural parameters such as micro-stress, dislocation densities, specific surface area are enhanced, which can be used to tailor the sensitivity accordingly.

Conclusions

Pristine and Ni doped TiO_2 thin films were successfully synthesized by spray pyrolysis technique on glass substrate with Ni dopant concentrations as 1, 2 and 4 *vol%.* Effects of the level of Ni dopant on structural, optical, electrical and humidity sensing properties of TiO_2 were successfully studied using appropriate techniques. XRD profile shows a small shift and reduction in intensity of the characteristic (101) peak with doping. It also confirms that the crystallite size decreases from 31 nm to 23 nm with increase in Ni doping percentage. From optical study, it is observed that the energy band gap decreases from 3.44 eV (pristine TiO_2) to 3.15 eV with Ni doping in TiO_2. The electrical resistance was observed to decline from 382 to 201 GΩ with rise in dopant concentration. Temperature coefficient of resistance and activation energy was also found to increase with the increase in doping level. Humidity sensing properties of the samples were also affected by the Ni dopant percentage and it was found that the sensitivity increases with the dopant concentration and was found to be maximum of 89 % for sample with 2 *vol%* of Ni doping in TiO_2. The minimum response time was observed to be 64.5 s for this sample.

Author Contribution:

Dipak L. Gapale – Research work, data curation and writing original draft; **Pravinkumar D. Jadhav** – Research work, prepared figures and some part of analysis; **Sainath R. Navale –** software, reviewing and editing of manuscript; **Balasaheb M. Palve –** Conceptualization, funding acquisition**; Sandeep A. Arote and Prashant K. Baviskar** – Formal Analysis, Supervision, Visualization & Conceptualization**.**

Clinical Trial Registration: *Not applicable.*

Consent to Participate Declarations: *Not applicable.*

Consent to Publish Declarations: *Not applicable.*

Ethics Declaration: Not applicable.

Conflicts of interest:

All authors read and approved the final manuscript. The authors declare that they have no conflict of interest.

Research involving Human Participants and/or Animals:

This manuscript does not contain any studies with human participants or animals performed by any of the authors.

Competing interests:

The authors have no competing interests to declare that are relevant to the content of this article.

Research Data Policy and Data Availability Statements:

All data generated or analyzed during this study are presented in the main manuscript.

References

[1] X. Yu, T. Marks, A. Facchetti, Metal oxides for optoelectronic applications, Nat. Mater. 15 (2016) 383.

[2] M. I. Uzzal, M. M. H. Bhuiyan, M. S. Manir, M. R. Amin, F. Mitsugi. Enhancing TiO_2-based dye-sensitized solar cell performance using Br_3^-/I^- electrolyte and natural dyes from pomegranate and teak leaves, Discov. Appl. Sci. 8 (2026) 181.

[3] A. V. Nimmy, V. M. Anandakumar, V. Biju. Enhancing the visible-light sensitive photocatalysis of anatase TiO_2 through surface-modification, Discov. Mater. 5 (2025) 45.

[4] M. Green, A.T. Van Tran, R. Smedley, A. Roach, J. Murowchick, X. Chen, Microwave absorption of magnesium/hydrogen-treated titanium dioxide nanoparticles, Nano Mater. Sci. 1 (2019) 48–59.

[5] D. Nunes, E. Fortunato, R. Martins, Flexible nanostructured TiO_2-based gas and UV sensors: A review, Discov. Mater. *2* (2022) 2.

[6] P. Su, Y. Sun, C. Lin, Novel low humidity sensor made of TiO_2 nanowires/poly(2-acrylamido-2-methylpropane sulfonate) composite material film combined with quartz crystal microbalance, Talanta. 69 (2006) 946–951.

[7] Y. Pi, B. Liu, Z. Li, Y. Zhu, Y. Li, F. Zhang, G. Zhang, W. Peng, X. Fan, TiO_2 Nanorod Arrays Decorated with Exfoliated WS_2 Nanosheets for Enhanced Photoelectrochemical Water Oxidation, J. Colloid Interface Sci. 545 (2019) 282.

[8] Q. Zhao, W. Wen, Y. Xia, J. Wu, Photocatalytic activity of TiO_2 nanorods, nanowires and nanoflowers filled with TiO_2 nanoparticles, Thin Solid Films 648 (2018) 103.

[9] O. Zakir, A. Ait-Karra, R. Idouhli, M. Khadiri, B. Dikici, A. Aityoub, A. Abouelfida, A. Outzourhit, A review on TiO_2 nanotubes: synthesis strategies, modifications, and applications. J. Solid State Electrochem. 27 (2023) 2289–2307.

[10] S. Kailasa, M. Sai Bhargava Reddy, B. Geeta Rani, K. Venkateswara Rao, K. Deshmukh, K. Kumar Sadasivuni, Highly sensitive electrochemical volatile organic compound (Acetone) sensing based on TiO_2 Nanocubes @Polyaniline nanostructure, Inorg. Chem. Commun. 157 (2023) 111420.

[11] H. Zhu, A. Haidry, Z. Wang, & Y. Ji, Improved acetone sensing characteristics of TiO_2 nanobelts with Ag modification, J. Alloys Compd., 887 (2021) 161312.

[12] S. Reghunath, D. Pinheiro, S. Devi KR, A review of hierarchical nanostructures of TiO_2: Advances and applications, Appl. Surf. Sci. Adv. 3 (2021) 100063.

[13] D. Gapale, S. Arote, R Borse, Mathematical Modeling of Droplet Formation, Evaporation, and Film Growth to Study Crystallite Size and Film Thickness of Spray Pyrolysis Deposited TiO_2 Thin Films, e-J. Surf. Sci. Nanotechnol. 16 (2018) 419.

[14] H. Peng, J. Li, S. Li, J. Xia, First-principles study of the electronic structures and magnetic properties of 3d transition metal-doped anatase TiO_2, J. Phys.: Condens. Matter. 20 (2008) 125207.

[15] L. Patle, V. Huse, A. Chaudhari, Band edge movement and structural modifications in transition metal doped TiO_2 nanocrystals for the application of DSSC, Mater. Res. Express. 4 (2017) 105045.

[16] S. Songara, L. Saini, G.S. Gowd, J.S. Rajpurohit, V. Gupta, M.K. Patra, S.R. Vadera, N. Kumar, Improved photochromic properties of W^{6+} doped nanostructured TiO_2 coatings, Results in Surfaces and Interfaces. 14 (2024) 100201.

[17] D. A. Hanaor, C. C. Sorrell, Review of the anatase to rutile phase transformation, J. Mater. Sci. 46 (2011) 855.

[18] M. Manzoor, A. Rafiq, M. Ikram, M. Nafees, S. Ali, Structural, optical, and magnetic study of Ni-doped TiO_2 nanoparticles synthesized by sol–gel method, Int. Nano Lett. 8 (2018) 1.

[19] S. Jensen, D. Kilin, Electronic properties of nickel-doped TiO_2 anatase, J. Phys.: Condens. Matter. 27 (2015) 134207.

[20] D. Jing, Y. Zhang, L. Guo, Study on the synthesis of Ni doped mesoporous TiO_2 and its photocatalytic activity for hydrogen evolution in aqueous methanol solution, Chem. Phy. Lett. 415 (2005) 74.

[21] N. Bahadur, K. Jain, A. Srivastava, Govind, R. Gakhar, D. Haranath, M. Dulat, Effect of nominal doping of Ag and Ni on the crystalline structure and photo-catalytic properties of mesoporous titania, Mater. Chem. Phy. 124 (2010) 600.

[22] R. L. Fomekong, K. Kelm, & B. Saruhan, High-Temperature Hydrogen Sensing Performance of Ni-Doped TiO_2 Prepared by Co-Precipitation Method, Sens. 20(21) (2020) 5992.

[23] H. Li, N. Li, Y. Zhang, H. He, Z. Liu, Visible light-induced super-hydrophilic anatase porous thin film with easy-to-clean and antifogging properties, J Sol-Gel Sci Technol. 83 (2017) 502.

[24] M. Morsy, M.M. Mokhtar, S.H. Ismail, G.G. Mohamed, M. Ibrahim, Humidity Sensing Behaviour of Lyophilized rGO/Fe2O3 Nanocomposite, J. Inorg. Organomet. Polym. Mater. 30 (2020) 4180–4190.

[25] Z. Li, A. Haidry, B. Gao, T. Wang, Z. Yao, The effect of Co-doping on the humidity sensing properties of ordered mesoporous TiO_2, Appl. Surf. Sci. 412 (2017) 638.

[26] M. Musa, M. Mamat, N. Vasimalai, I. Banu, N. Parimon, H. Hassan, M. Malek, M. Rusop, Humidity Sensing Performance of V: TiO_2 3D Nanostructure based Humidity Sensor, IOP Conf. Ser. Earth Environ. Sci. 682 (2021) 012073.

[27] N. K. Pandey, K. Tiwari, A. Roy, ZnO–TiO_2 nanocomposite: Characterization and moisture sensing studies, Bull. Mater. Sci. 35 (2012) 347.

[28] M. Sudha, S. Radha, S. Kirubaveni, R. Kiruthika, R. Govindaraj, N. Santhosh, Experimental study on structural, optoelectronic and room temperature sensing performance of Nickel doped ZnO based ethanol sensors, Solid State Sci. 78 (2018) 30–39.

[29] P. Hermawan, H. Pranowo, I. Kartini, Physical characterization of Ni(II) Doped TiO_2 Nanocrystal by Sol-Gel Process, Indo. J. Chem. 11 (2011) 135.

[30] D. Gapale, S. Arote, B. Palve, S. Dalvi, R. Borse, Effect of film Thickness on Humidity Sensing of Spray Deposited TiO_2 Thin Films, Mater. Res. Express. 6 (2019) 026402.

[31] M. Shaban, A. Ahmed, N. Shehata, M. Betiha, A. Rabie, Ni-doped and Ni/Cr co-doped TiO_2 nanotubes for enhancement of photocatalytic degradation of methylene blue, J. Colloid Interface Sci. 555 (2019) 31.

[32] B. Gao, T. Wang, X. Fan, H. Gong, H. Guo, W. Xia, Y. Feng, X. Huang, J. He, Synthesis of yellow mesoporous Ni-doped TiO_2 with enhanced photoelectrochemical performance under visible light. Inorg, Chem. Front. 4 (2017) 898.

[33] X. Yang, H. Fu, L. Zhang, X. An, S. Xiong, X. Jiang, A. Yu, Enhanced gas sensing performance based on the fabrication of polycrystalline Ag@TiO_2 core-shell nanowires, Sens. Actuators B chem. 286 (2019) 483.

[34] N. I. Beedri, P. K. Baviskar, A. T. Supekar, Inamuddiny, S. R. Jadkar, H. M. Pathan, Bilayered ZnO/Nb_2O_5 photoanode for dye sensitized solar cell, Int. J. Mod. Phys. B 32 (2018) 1840046

[35] T. Jianjun, H. Gao, H. Deng, L. Sun, H. Kong, P. Yang, J. Chu, Structural, magnetic and optical properties of Ni-doped TiO_2 thin films deposited on silicon (100) substrates by sol–gel process, J. Alloys Compd. 581 (2013) 318.

[36] T. Nishikawa, T. Nakajima, Y. Shinohara, An exploratory study on effect of the isomorphic replacement of Ti^{4+} ions by various metal ions on the light absorption character of TiO_2, J. Mol. Struct. THEOCHEM. 545 (2001) 67.

[37] L. Li, Z. Wu, Y. Ju, C. Chen, Process Effects on Heat-Sensitive Properties of Sputtered TiOx Thin Film, Energy Procedia. 12 (2011) 456.

[38] H. Farahani, R. Wagiran, M. Hamidon, Humidity Sensors Principle, Mechanism, and Fabrication Technologies: A Comprehensive Review, Sens. 14 (2014) 7881.

[39] Z. Li, A. A. Haidry, B. Gao, T. Wang, Z. Yao, The effect of Co-doping on the humidity sensing properties of ordered mesoporous TiO_2, Appl. Surf. Sci. 412 (2017) 638.

[40] D. Toloman, A. Popa, M. Stan, C. Socaci, A. R. Biris, G. Katona, F. Tudorache, I. Petrila, F. Iacomil, Reduced graphene oxide decorated with Fe doped SnO_2 nanoparticles for humidity sensor, Appl. Surf. Sci. 402 (2017) 410.

[41] K. Rathi, K. Pal, Impact of Doping on GO: Fast Response−Recovery Humidity Sensor, ACS Omega 2 (2017) 842.

[42] I. Popov, Z. Zhu, A.R. Young-Gonzales, R.L. Sacci, E. Mamontov, C. Gainaru, S.J. Paddison, A.P. Sokolov, Search for a Grotthuss mechanism through the observation of proton transfer, Commun. Chem. 6 (2023) 77.

[43] D. Gapale, S. Arote, B. Palve, & R. Borse, Influence of precursor solution concentration on the structural, optical and humidity sensing properties of spray-deposited TiO_2 thin films, J. Semicond. 39(12) (2018) 122003.

[44] Z. Li, A.A. Haidry, B. Gao, T. Wang, Z. Yao, The effect of Co-doping on the humidity sensing properties of ordered mesoporous TiO_2, Appl. Surf. Sci. 412 (2017) 638–647.

[45] Z. Li, A. Haidry, B. Dong, L. Sun, Q. Fatima, L. Xie, Z. Yao, Facile synthesis of nitrogen doped ordered mesoporous TiO_2 with improved humidity sensing properties, J. Alloys Compd. 742 (2018) 814.

[46] Q. Qi, T. Zhang, L. Wang, Improved and excellent humidity sensitivities based on KCl doped TiO_2 electrospun nanofibers, Appl. Phys. Lett. 93 (2008) 023105.

[47] W. Li, M. Hu, P. Ge, J. Wang, Y. Guo, Humidity sensing properties of morphology controlled ordered silicon nanopillar, Appl. Surf. Sci. 317 (2014) 970.

[48] D. Das, Y. Yang, J. O'Brien, D. Breznan, S. Nimesh, S. Bernatchez, M. Hill, A. Sayari, R. Vincent, and P. Kumarathasan, Synthesis and Physicochemical Characterization of Mesoporous Nanoparticles, J. Nanomater. (2014) 1.

[49] M. N. Solovan, P. D. Maryanchuk, V.V. Brus, O. A. Parfenyuk, Electrical and Optical Properties of TiO_2 and TiO_2:Fe Thin Films, Inorg Mater. 48 (2012) 1154.

Table Captions:

Table 1: Structural parameters like crystallite size, microstrain and specific surface area for pristine and Ni doped TiO_2 thin films.

Table 2: Elemental data from EDX spectrum and direct optical band gap for pristine and Ni doped TiO_2 thin films.

Table 3: Electrical resistance, TCR and activation energy for pristine and Ni doped TiO_2 thin films.

Table 4: Sensitivity, response, recovery time and hysteresis loss for pristine and Ni doped TiO_2 thin films.

Table 1

Sample	Ni *vol%*	Crystallite size (nm)	Micro-strain ($\times 10^{-3}$)	Specific surface area (m^2/g)
Pristine TiO_2	0	31	1.76	49
1% Ni :TiO_2	1	24	2.48	65
2% Ni : TiO_2	2	23	2.6	66
4% Ni : TiO_2	4	27	2.3	56

Table 2

Sample	Ni *vol%*	Oxygen *at%* (%)	Titanium *at%* (%)	Ni *at%* (%)	Band gap (eV)
Pristine TiO_2	0	81.08	18.92	--	3.44 [34]
1% Ni :TiO_2	1	84.14	15.16	0.70	3.25
2% Ni : TiO_2	2	85.00	13.86	1.14	3.15
4% Ni :TiO_2	4	86.25	12.18	1.57	3.23

Table 3

Sample	Ni *vol %*	Resistance (GΩ)	Temp. coefficient of resistance (TCR) ($\times 10^{-3}$) (/°C)	Activation energy (Ea) (eV)
Pristine TiO_2	0	382	-1.4	0.34
1% Ni : TiO_2	1	342	-1.5	0.36
2% Ni : TiO_2	2	250	-1.72	0.44
4% Ni : TiO_2	4	201	-1.78	0.66

Table 4

Sample	Ni *Vol%*	Sensitivity at 90% RH (%)	Response Time (s)	Recovery time (s)	% of Hysteresis (%)
Pristine TiO_2	0	83.7	77.5	3.5	1.19
1% Ni : TiO_2	1	85.5	70	3	1.61
2% Ni : TiO_2	2	89.0	64	3	4.18
4% Ni : TiO_2	4	80.5	120.5	4.5	6.37

Figure Captions:

Figure 1: XRD patterns for pristine and Ni doped TiO_2 thin films annealed at 500 ^oC.

Figure 2: SEM image for (P) pristine TiO_2, 1*%* Ni :TiO_2, 2*%* Ni :TiO_2 and 4*%* Ni : TiO_2 thin films.

Figure 3: EDX spectrum of (P) pristine TiO_2, (NT1) 1 *vol%* Ni-TiO_2, (NT2) 2 *vol%* Ni-TiO_2 and (NT4) 4 *vol%* Ni-TiO_2 thin films.

Figure 4: Variation of square of absorbance with photon energy for the calculations of optical band gap for the samples pristine and Ni doped TiO_2. Inset shows the schematic of energy level diagram of pristine and Ni doped TiO_2 samples.

Figure 5: Variation of log(R_a) with temperature to calculated TCR for Ni doped TiO_2 thin film.

Figure 6: Variation of log(Ra) with 1000/T to calculate activation energy for pristine and Ni doped TiO_2 thin films.

Figure 7: Variation of resistance with relative humidity for Ni doped TiO_2 thin films.

Figure 8: Hysteresis loops for pristine and Ni doped TiO_2 thin films.

Figure 9: Variation of resistance with time to calculate response and recovery time for Ni doped TiO_2 thin films.

Figure 10: Variation in sensitivity and response time with different Ni *vol%* for Ni doped TiO_2 thin films.

Figure 1

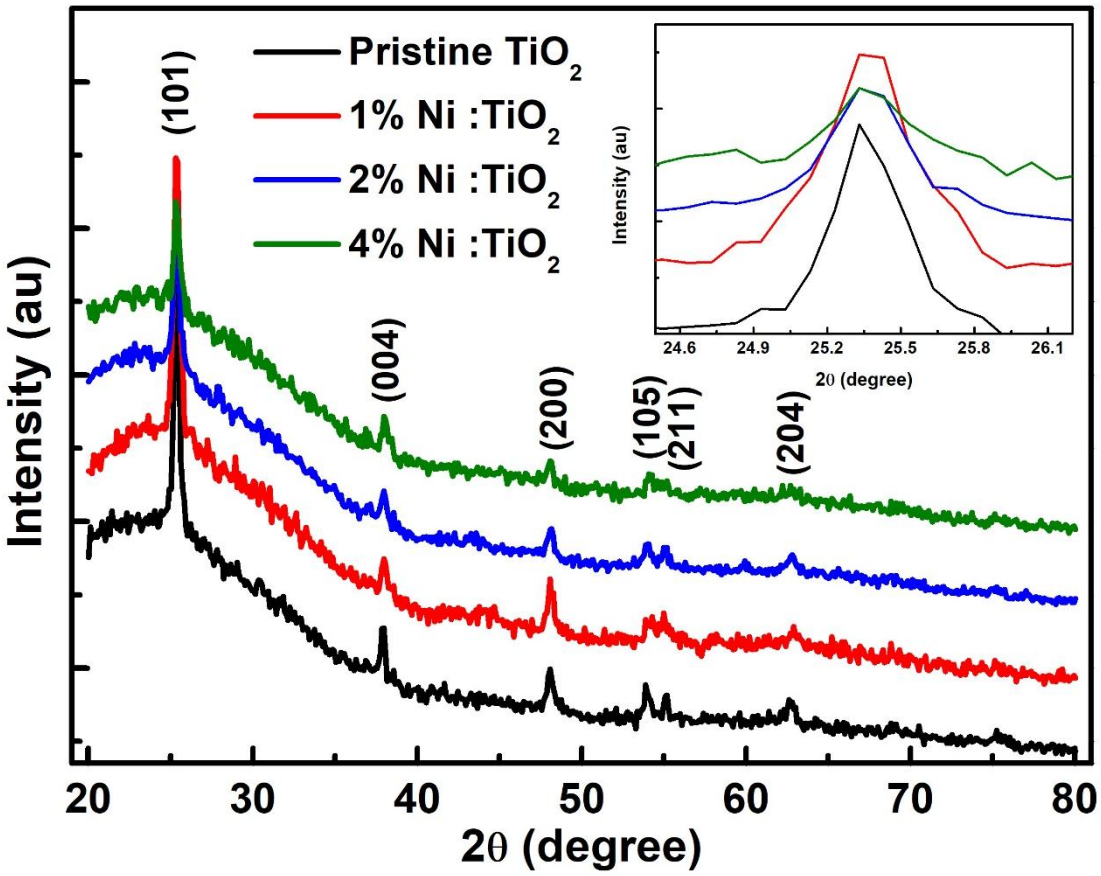

Pristine TiO2
1% Ni :TiO2
2% Ni :TiO2
4% Ni :TiO2
(101)
(004)
(200)
(105)
(211)
(204)
Intensity (au)
2θ (degree)
20
30
40
50
60
70
80
Intensity (au)
24.6
24.9
25.2
25.5
25.8
26.1
2θ (degree)

Figure 2

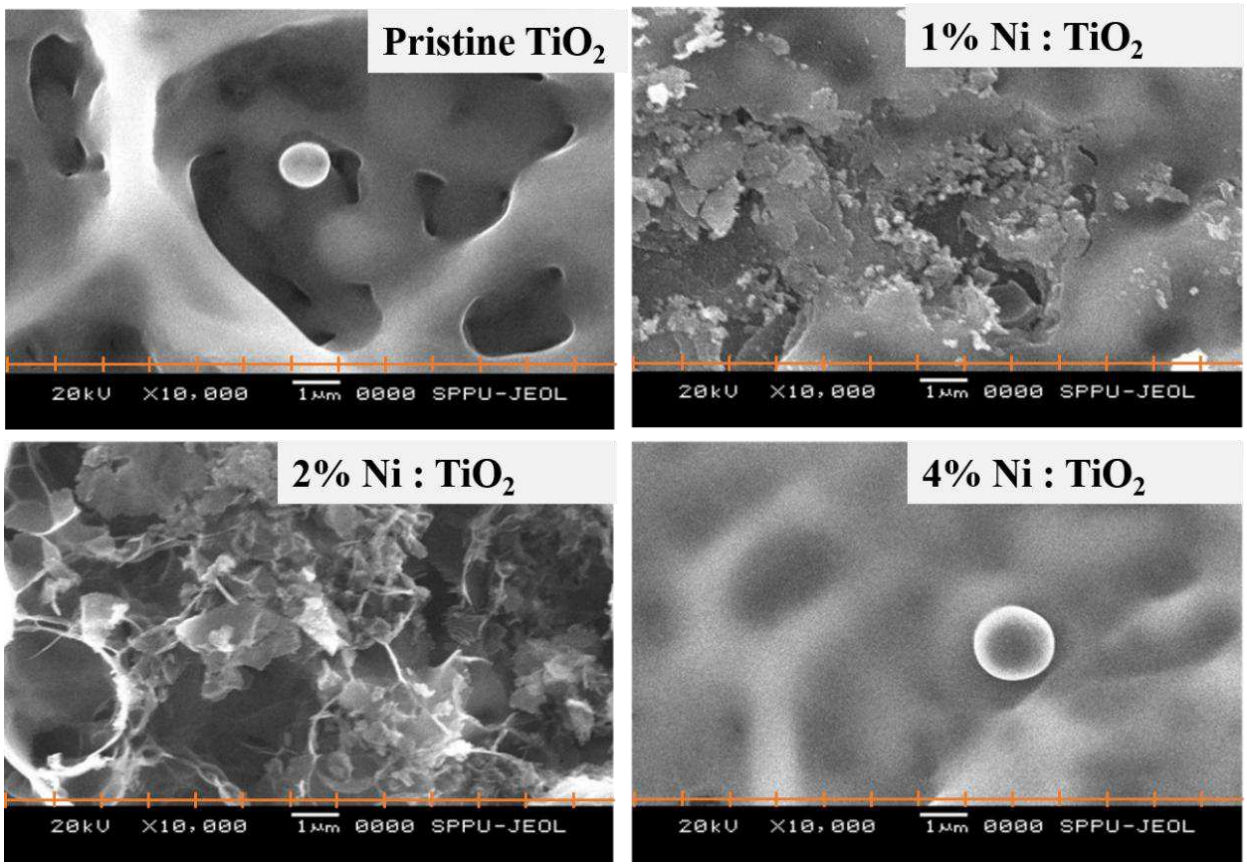

Pristine TiO_2
20kV X10,000 1μm 0000 SPPU-JEOL
1% Ni : TiO_2
20kV X10,000 1μm 0000 SPPU-JEOL
2% Ni : TiO_2
20kV X10,000 1μm 0000 SPPU-JEOL
4% Ni : TiO_2
20kV X10,000 1μm 0000 SPPU-JEOL

Figure 3

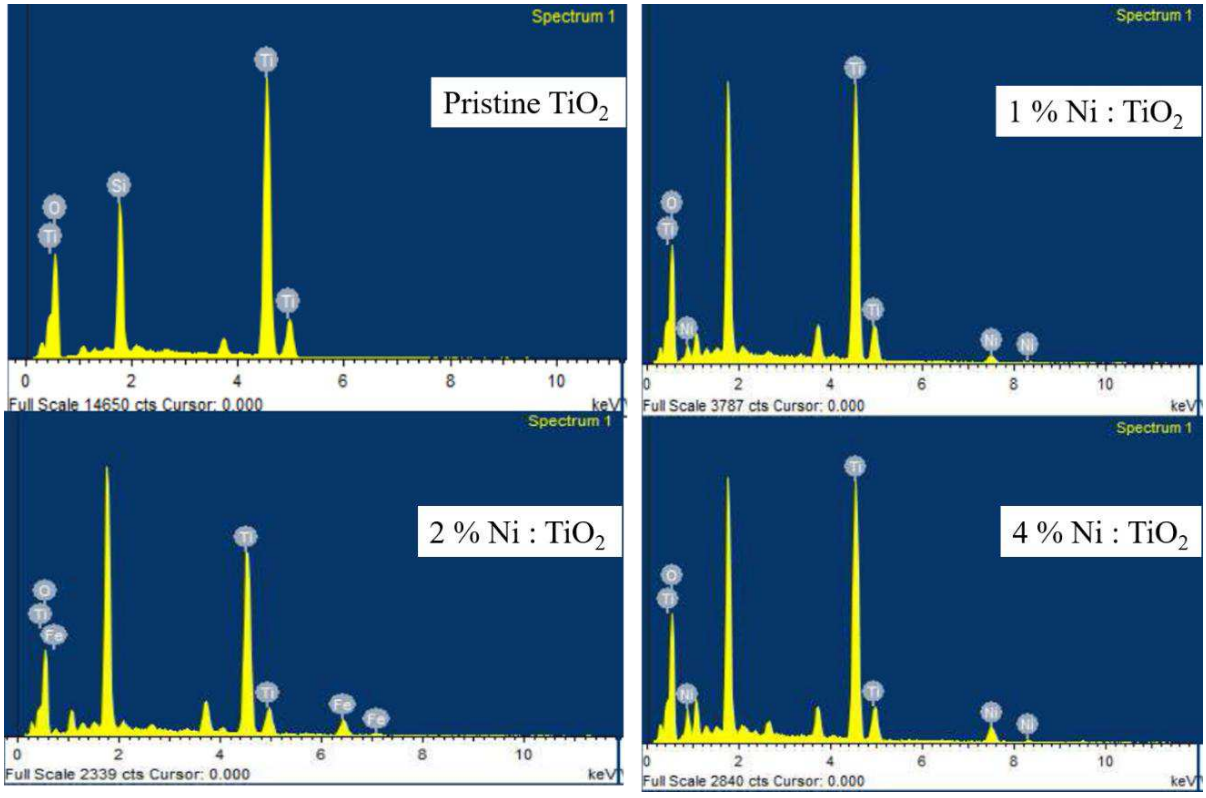

Spectrum 1
Pristine TiO_2
O
Si
Ti
Ti
0 2 4 6 8 10
Full Scale 14650 cts Cursor: 0.000
keV
Spectrum 1
1 % Ni : TiO_2
O
Ti
Ti
Ni
Ni
Ni
0 2 4 6 8 10
Full Scale 3787 cts Cursor: 0.000
keV
Spectrum 1
2 % Ni : TiO_2
O
Ti
Fe
Ti
Ti
Fe
Fe
0 2 4 6 8 10
Full Scale 2339 cts Cursor: 0.000
keV
Spectrum 1
4 % Ni : TiO_2
O
Ti
Ti
Ni
Ti
Ni
Ni
0 2 4 6 8 10
Full Scale 2840 cts Cursor: 0.000
keV

Figure 4

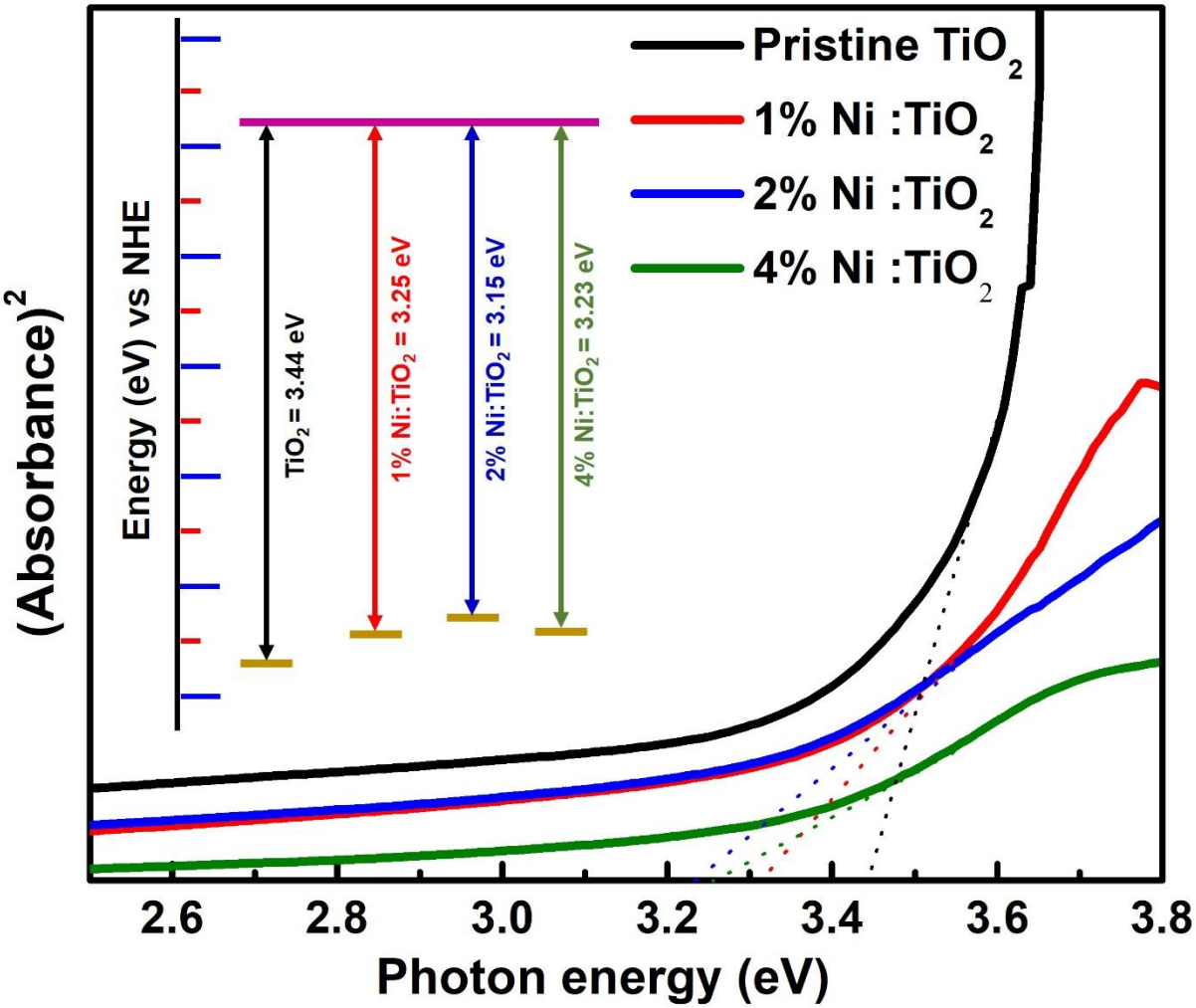

Pristine TiO2
1% Ni :TiO2
2% Ni :TiO2
4% Ni :TiO2
Energy (eV) vs NHE
TiO2 = 3.44 eV
1% Ni:TiO2 = 3.25 eV
2% Ni:TiO2 = 3.15 eV
4% Ni:TiO2 = 3.23 eV
(Absorbance)2
2.6
2.8
3.0
3.2
3.4
3.6
3.8
Photon energy (eV)

Figure 5

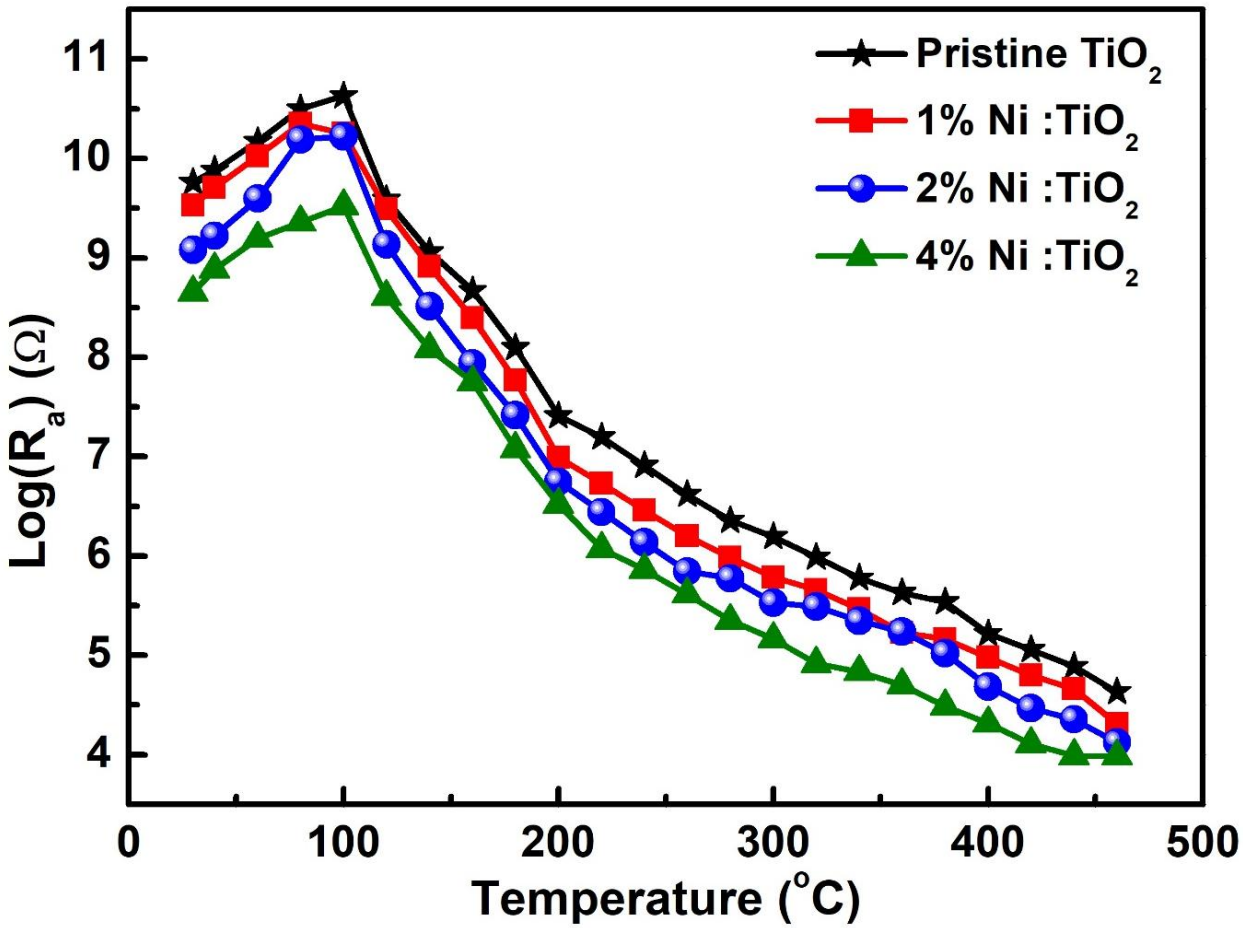

Pristine TiO2
1% Ni :TiO2
2% Ni :TiO2
4% Ni :TiO2
Log(Ra) (Ω)
Temperature (°C)
11
10
9
8
7
6
5
4
0
100
200
300
400
500

Figure 6

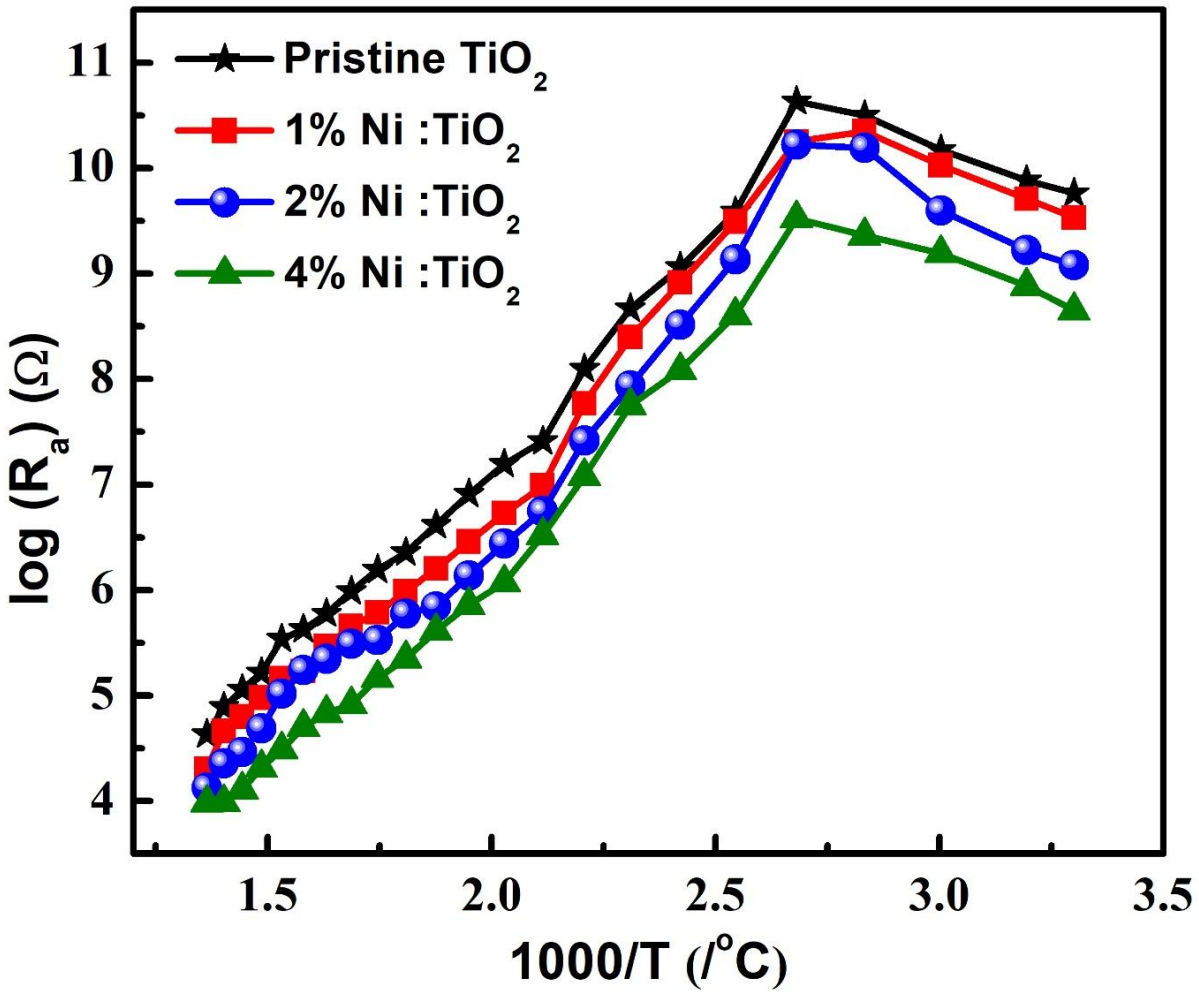

Pristine TiO2
1% Ni :TiO2
2% Ni :TiO2
4% Ni :TiO2
log (Ra) (Ω)
1000/T (/°C)
11
10
9
8
7
6
5
4
1.5
2.0
2.5
3.0
3.5

Figure 7

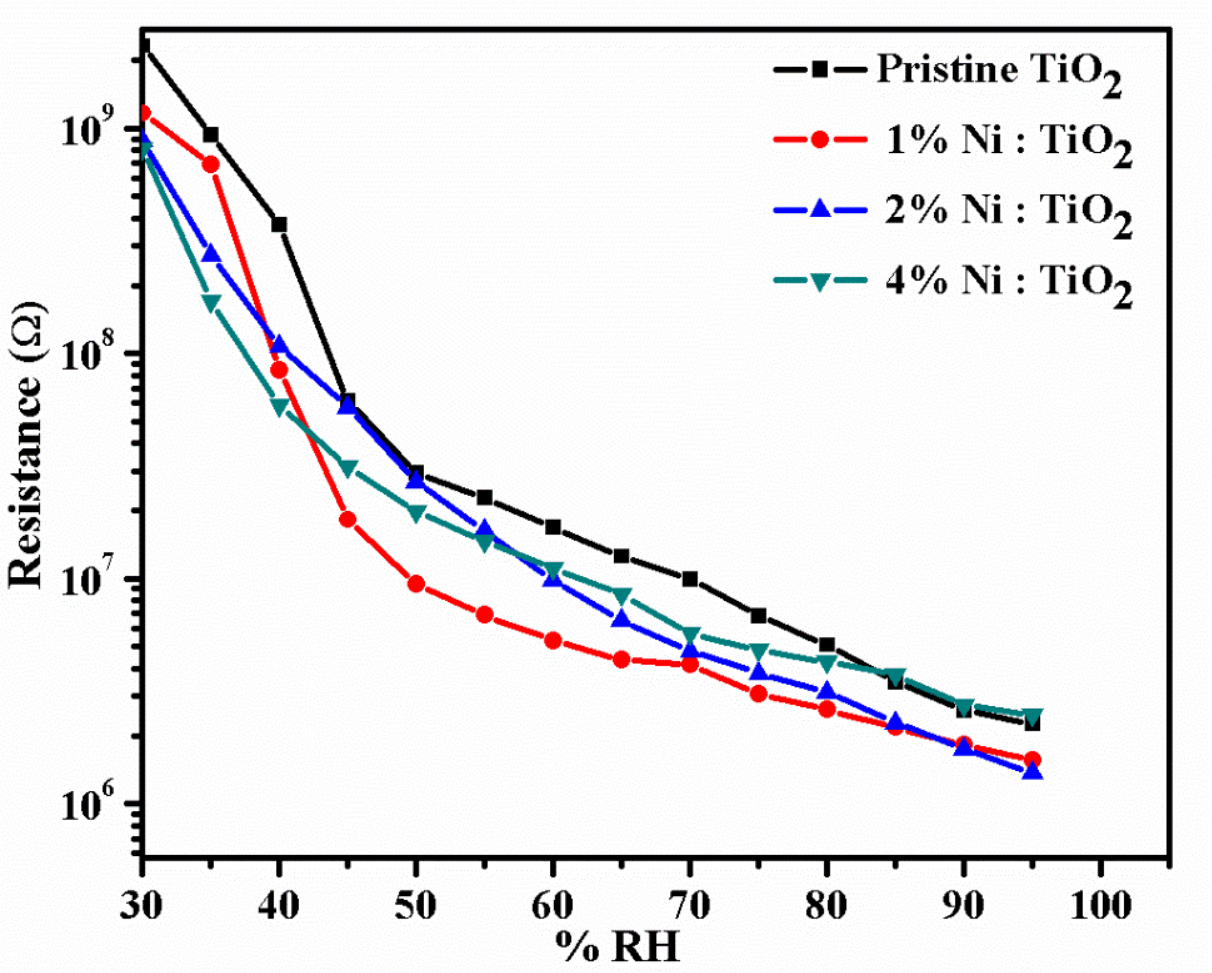

Pristine TiO2
1% Ni : TiO2
2% Ni : TiO2
4% Ni : TiO2
Resistance (Ω)
10^9
10^8
10^7
10^6
30
40
50
60
70
80
90
100
% RH

Figure 8

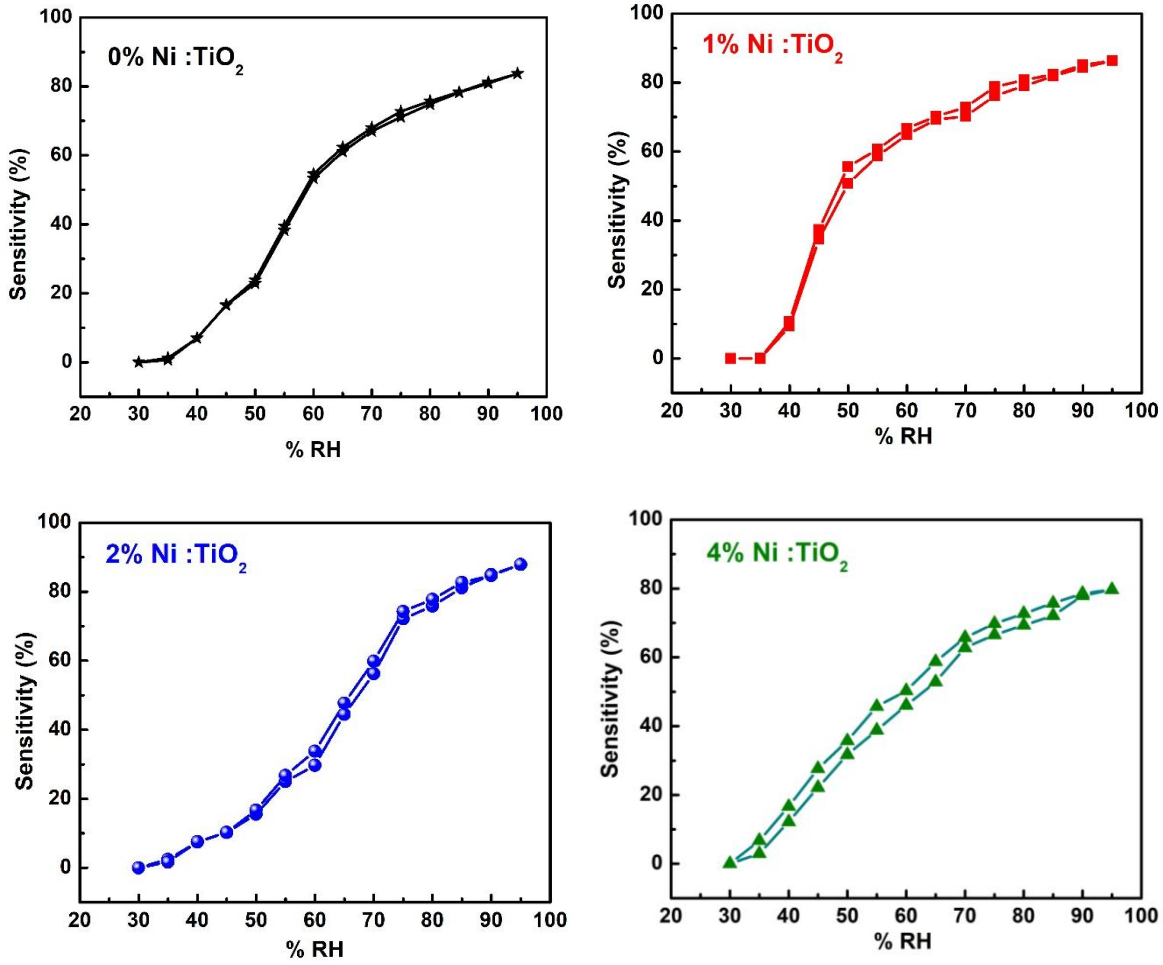

0% Ni :TiO2
1% Ni :TiO2
2% Ni :TiO2
4% Ni :TiO2
Sensitivity (%)
% RH
20
30
40
50
60
70
80
90
100
0
20
40
60
80
100

Figure 9

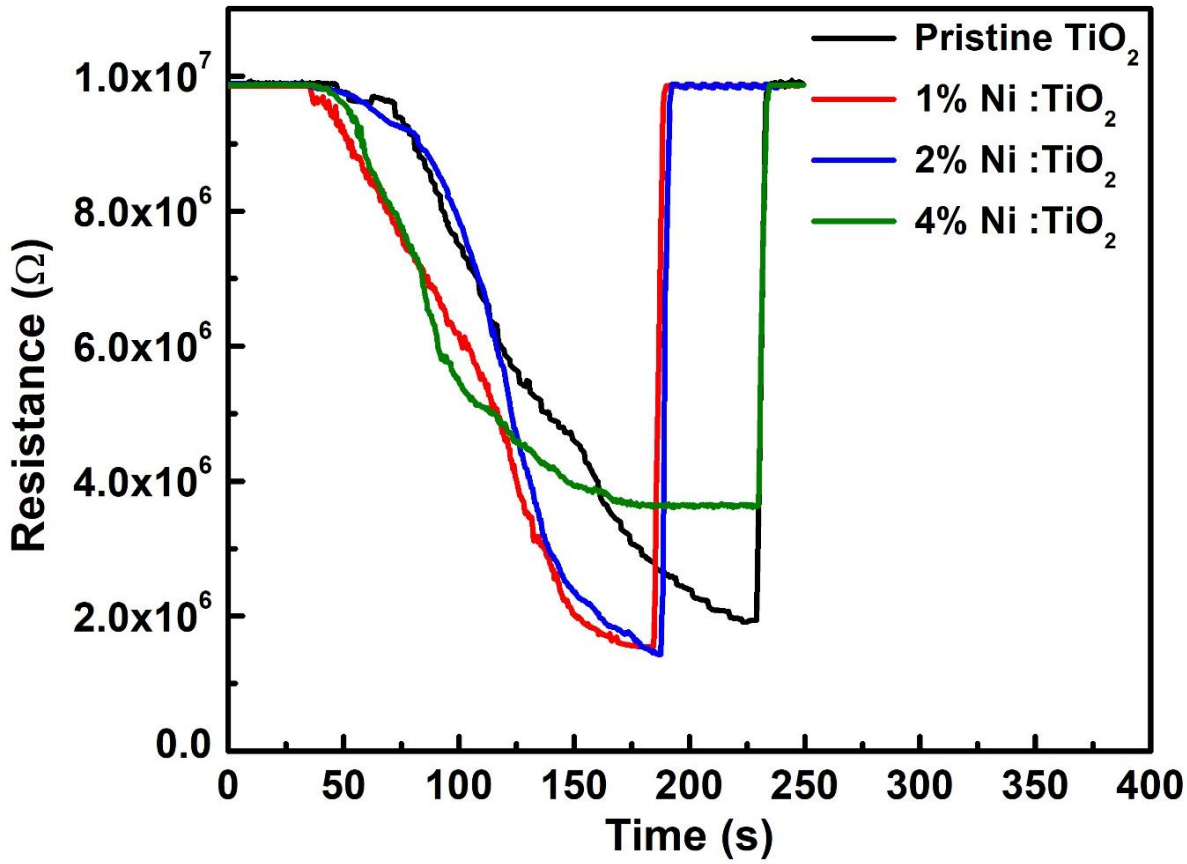
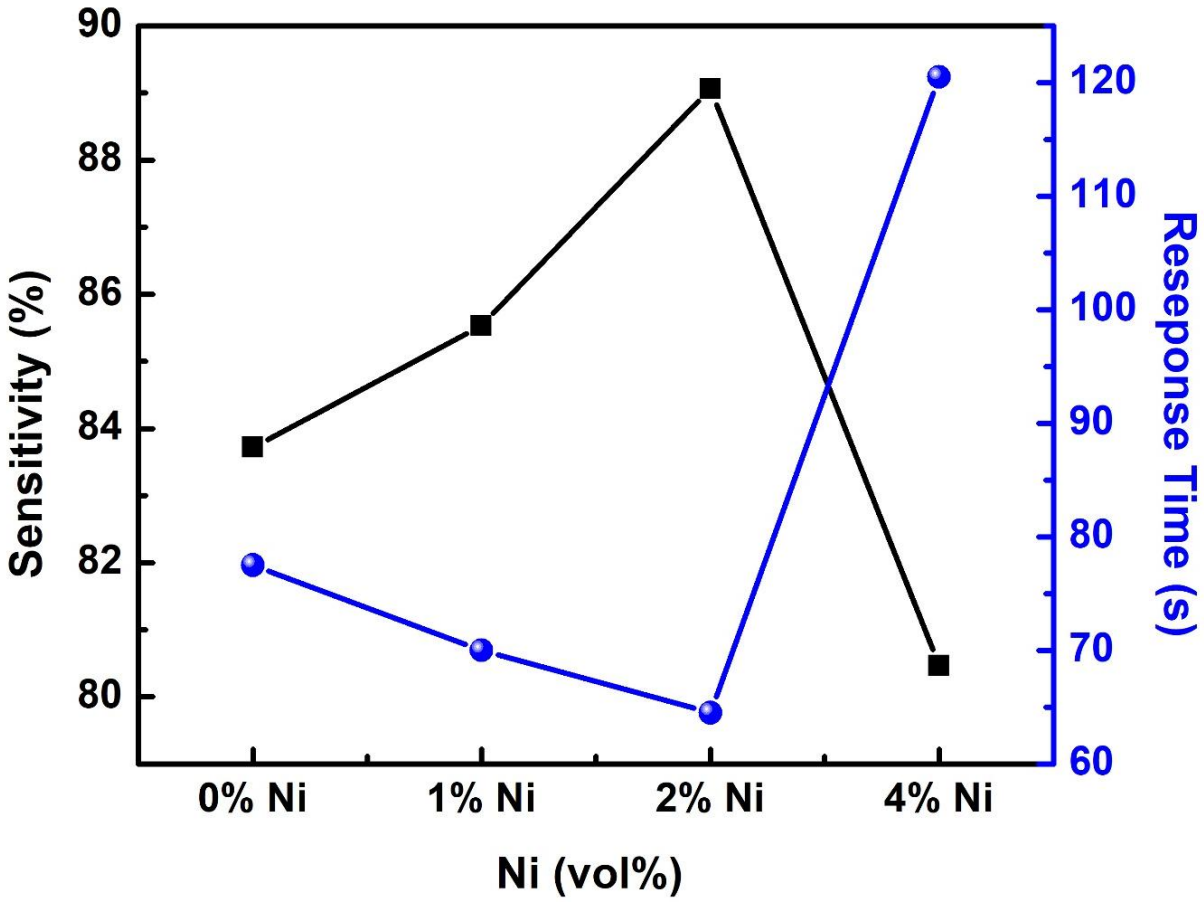

Pristine TiO2
1% Ni :TiO2
2% Ni :TiO2
4% Ni :TiO2
Resistance (Ω)
1.0x10^7
8.0x10^6
6.0x10^6
4.0x10^6
2.0x10^6
0.0
0
50
100
150
200
250
300
350
400
Time (s)

Figure 10


Sensitivity (%)
Response Time (s)
Ni (vol%)
0% Ni
1% Ni
2% Ni
4% Ni
90
88
86
84
82
80
120
110
100
90
80
70
60

Supplementary Files

This is a list of supplementary files associated with this preprint. Click to download.

- Highlights.docx
- NoveltyStatement.docx